JAST, Vol. 14, No. 2, pp. 31-51

JAST
Journal of Aerospace Science and Technology

Science Article

Study on effects of different rotational speed functions in elastic-plastic analysis of annular thin disk of functionally graded material

Hadi Hamedani [1], Ahmad Mamandi [2*]

1-2. Department of Mechanical Engineering, Parand Branch, Islamic Azad University, Parand, Iran

[*]**Email: am_2001h@yahoo.com**

In this paper, the effects of different rotational speed functions in the elastic-plastic deformation and stress analysis of a rotating annular thin disk of functionally graded material (FGM) in Reddy model is studied using the analytical and FEM methods. In this regard, differential equations governing dynamic equilibrium for displacements and stresses in the elastic region of the FGM rotating disk have been derived using the theory of elasticity in plane stress condition and have been solved by the shooting method. Then, the equations governing the distribution of plastic radial and circumferential stresses on the disk have been extracted using the Prandtl-Reuss theory of plasticity and based on the Ludwig hardening law in conjunction with the von Mises yield criterion. Also, by modeling the annular thin disk in the environment of finite element software ANSYS, the results obtained from the elastic analytical solution and the finite element numerical solution have been compared to each other and to the results reported in the literature for specific cases and validated accordingly. The effects of variation of the disk geometric parameters, functionally graded material power index as well as different type of the time-dependent rotational speed functions such as the constant speed, exponential, and accelerated/decelerated linear, quadratic, and square root functions on the elastic behavior of the disk and distribution of radial displacement, and also distribution of radial, circumferential, and shear stresses on the disk have been studied. Moreover, the results of plastic analysis have been presented for distribution of radial and circumferential stresses on the disk.

Keywords: *Annular FGM rotating thin disk, Accelerated/decelerated rotational speed, Elastic-plastic analysis, Ludwig hardening law, von Mises yield criterion.*

Introduction

Nowadays with the development of research works and new technologies, the recognition and use of new materials in industries has been more important. In this regard, industrial and academic research have given special attention to the recognition, production, and development of new materials including composite materials, shape memory alloys, piezoelectric materials, nano materials, and functionally graded materials (FGMs). Since the rapid development of technology requires the use of new materials as a priority of engineering in complex systems with high efficiency, the use of functionally graded materials has increased in recent years. The application of these materials has received more attention in the missile industry, the aerospace industry in gas turbines, reactors, and in other cases where the high strength, low density, and thermal resilience of material are of great

1. M.Sc. graduate
2. Associate Professor (Corresponding Author)

Receiced: 12 October 2020
Accepted: 27 April 2021

importance. Rotating disks are widely used in rotatory equipments. These spinning disks experience different speeds in actual operating conditions during start-up, shut down, full load, or partial load operations. Therefore, during operation in a steady or transient state, they have different levels of generated stresses and dynamic behaviors accordingly. Also, due to high stress levels arising from mechanical or thermo-mechanical loading involving the centrifugal force, stress beyond the elastic limit can be created in them. Therefore, it is important to investigate and to analyze the elasto-plastic behavior of the FGM rotating disk. In the field of elastic analyses of the FGM rotating disks, we can refer to references [1-10]. Moreover, a number of research works conducted in the field of rotating disk analysis have been investigated in the following. The 3D elastic behavior of the FGM rotating disk investigated in [11]. By extending the 2D plane stress problem to a three-dimensional problem, they showed that the plane stress solution satisfies all of three dimensional equations governing the motion of disk but it is not able to yield any results in an adaptive 3D strain field. In [12] and [18], the elasto-plastic stress behavior of the FGM rotating disks with constant rotating velocity has been analyzed. In these studies, the yielding behavior of the disk is considered without any hard working process on the material. It was considered the modulus of elasticity, density, and yield strength as a power distribution function and different rotating velocities to examine the distribution of plastic regions was used. Then, the distribution of radial and circumferential stresses in the rotating disk determined. In [13] and [14] the elastic analysis of orthotropic disks made of functionally graded materials was studied and the effects of orthotropic feature and corresponding changes on the elastic field, particularly the distribution of circumferential stresses created in hollow rotary disks with constant rotating velocity has been investigared. The analysis of the thick rotating disk with variable thickness and with the varying properties of functionally graded material in 2D state was conducted in [15]. In [16], the exact solution of the elastic-perfectly plastic deformation of the solid rotating disk made of functionally graded material was investigated. A semi-analytical solution for stress-strain equation based on the von Mises non-linear yield criterion according to the rules of yielding on the disk was obtained. The solution was obtained for a rotating disk containing a plastic core. In [17], the elasto-plastic behavior of a rotating disk made of functionally graded material has been studied. Using closed form and exact solution of the problem, the elasto-plastic strain and displacements of a FGM rotating disk based on the elastic-perfectly plastic model and Tresca yield criterion was obtained. Elastic analysis for displacement and stress distribution in a FGM rotating circular disk with a variable angular speed was studied in [18]. The elastic modulus and the rotating disk density considered as variable parameters along the radius of the disk and proportional to the volume fraction of materials. The motion equations of the FGM rotating circular disk had been simplified into boundary value problem of ordinary differential equation and were solved using the shooting method. Numerical results show that the functionally graded index, angular speeds, and geometric shape all have significant effect on the mechanical behaviors of the rotating FGM circular disk. Elastic–plastic stress analysis of FGM disks subjected to constant angular velocity investigated in [19] considering yielding behavior of the disk material follows to be non-work hardening case. Elasticity modulus, density and yield strength of the disk vary radially according to a power law function. Radial and tangential stress components are obtained for angular velocities and gradient parameters with different values. Stress analysis in FGM disks with non-uniform thickness and variable angular velocity has been studied in [20]. Elastic-plastic analysis of pressure vessels and rotating disks made of functionally graded materials using the isogeometric approach has been analyzed in [21]. It is assumed that the material plastic deformation follows an isotropic strain-hardening rule based on the von Mises yield criterion. Numerical solution of thermal elastic-plastic functionally graded thin rotating disk with exponentially variable thickness and variable density has been investigated in [22]. In the present study, the elastic-plastic deformation and stress analysis of an annular disk of functionally graded materials (FGM) is investigated using analytical method. The properties of FGM are assumed to be varied by a power distribution continuous function in the Reddy model along the disk radius and do not change along the disk thickness. Also, rotational speed is considered as time-dependent variable functions, such as constant velocity function, exponential function, accelerated/decelerated

linear function, quadratic function, and square root function. In this regard, using differential equations of dynamic equilibrium, the equations governing the elastic displacements and stresses of the FGM rotating disk are derived using the elasticity theory in the plane stress state and are solved by the shooting method. Then, using the Prandtl-Reuss theory of plasticity and based on Ludwig hardening law via von Mises yield criterion, the equations governing the distribution of radial and circumferential plastic stresses in the disk have been derived accordingly. The effect of changes of the geometric parameters of the disk, the power index of functionally graded material and rotating velocity function is investigated in radial displacement and radial, circumferential, and shear elastic stresses as well as radial and circumferential plastic stresses in the rotating disk. Also, by modeling the annular disk, applying boundary conditions and mechanical properties, meshing, applying initial conditions in the environment of finite element software ANSYS, the results of numerical solution obtained using the finite element method (FEM) and the obtained results from elastic analytical and numerical methods are compared to each other and to the results reported in the literature for special cases of the problem. It should be pointed out that the more contribution and significant advantages of this paper are to present some results that have not been reported in the earlier published papers.

Modeling and deriving the governing equations in the elastic and plastic regions of the annular rotating thin disk

In Fig. 1, the annular hollow disk made from functionally graded material with inner radius a and the outer radius b has been shown in the cylindrical coordinate system $Or\theta z$ where O is the origin of coordinate system and r, θ, and z are the radial, circumferential, and longitudinal coordinates, respectively. It is assumed that the disk rotates around the longitudinal axis z with an arbitrary angular speed function of time t, i.e., $\omega(t)$. It is also assumed that the properties of FGM disk including elastic modulus $E(r)$, density $\rho(r)$, and yield stress $\sigma_y(r)$ are varied continuously in radial direction. Also, the Poisson's ratio v is assumed to be constant.

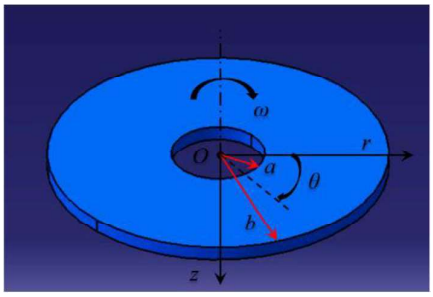

Fig. 1: The FGM rotating annular thin disk and the cylindrical coordinate system $r\theta z$

The properties of functionally graded material, P, using Reddy model are considered as a power function (with the power or index of functionally graded material n) with volumetric distribution in Eq. (1), where, P_m and P_c are the physical properties of metal and ceramic, respectively [19]. Also, V_m and V_c are the volumetric distribution of the ceramic and metal materials, respectively, which vary with a power function [18]

$$P = P_c V_c + P_m V_m,$$
$$V_c + V_m = 1,\ V_m = \left(\frac{r-a}{b-a}\right)^n,\ 0 < n < \infty \tag{1}$$

The general, property P, which indicates the variation of the physical properties such as elasticity modulus, density, and yield stress in r direction can be rewritten as follows

$$P = P_c\left[1-\left(\frac{r-a}{b-a}\right)^n\right] + P_m\left(\frac{r-a}{b-a}\right)^n,$$
$$\Rightarrow P = (P_m - P_c)\left(\frac{r-a}{b-a}\right)^n + P_c, \tag{2}$$

Dynamic equilibrium equations

By neglecting the gravitational force, only body forces are applied in the form of the radial centrifugal force $f_r = \rho(r).r.\omega(t)^2$ and the circumferential force $f_\theta = -\rho(r).r.\frac{d\omega(t)}{dr}$ on the rotating disk. Due to the fact that the disk radius is much larger than its thickness ($R >> t$), for the plane stress state, the disk dynamic equilibrium equations in radial and circumferential directions are as follows [18, 19, and 20]

$$\frac{\partial\sigma_r(r,t)}{\partial r} + \frac{\partial\tau_{r\theta}(r,t)}{r\partial\theta} + \frac{\sigma_r(r,t)-\sigma_\theta(r,t)}{r} + \rho(r)r\omega(t)^2 = 0, \tag{3}$$

$$\frac{\partial\sigma_\theta(r,t)}{r\partial\theta} + \frac{\partial\tau_{r\theta}(r,t)}{\partial r} + \frac{2\tau_{r\theta}(r,t)}{r} - \rho(r)r\frac{d\omega(t)}{dt} = 0, \tag{4}$$

where σ_r, σ_θ, and $\tau_{r\theta}$ are radial, circumferential, and planar shear stresses, respectively.

Strain-displacement equations

The strain-displacement equations are as follows [18, 19, and 20]

$$\varepsilon_r(r,t)=\frac{\partial u_r(r,t)}{\partial r}, \tag{5}$$

$$\varepsilon_\theta(r,t)=\frac{u_r(r,t)}{r}+\frac{1}{r}\frac{\partial u_\theta(r,t)}{\partial \theta}, \tag{6}$$

$$\gamma_{r\theta}=\frac{1}{r}\frac{\partial u_\theta}{\partial \theta}+\frac{\partial u_\theta}{\partial r}-\frac{u_\theta}{r}, \tag{7}$$

where ε_r, ε_θ, and $\gamma_{r\theta}$ are radial strain, circumferential strain, and shear strain, respectively. Also, u_r is the radial displacement and u_θ is the circumferential displacement in the $r\theta$ plane.

Stress-strain equations

The plane stress-strain equations are as follows [18, 19, and 20]

$$\varepsilon_r(r,t)=\frac{\partial u_r(r,t)}{\partial r}, \tag{8}$$

$$\varepsilon_\theta(r,t)=\frac{u_r(r,t)}{r}+\frac{1}{r}\frac{\partial u_\theta(r,t)}{\partial \theta}, \tag{9}$$

$$\gamma_{r\theta}=\frac{1}{r}\frac{\partial u_\theta}{\partial \theta}+\frac{\partial u_\theta}{\partial r}-\frac{u_\theta}{r}, \tag{10}$$

where

$$c_1=\frac{v}{1-v^2},\ c_2=\frac{1}{1-v^2} \tag{11}$$

In these equations, $E(r)$ is the elastic modulus that varies along the disk radius; c_1 and c_2 are the constant coefficients in terms of the Poisson ratio v. According to the axisymmetric condition of the rotating disk, the displacement of the disk is independent of the angle θ and depends only on the radial coordinate of the disk, r, and time t, i.e., and $u_r = u_r(r, t)$ and $u_\theta = u_\theta(r, t)$. By substituting Eqs. (5) to (7) in Eqs. (8) to (10) and noting that derivation with respect to θ, i.e., $\partial(\,)/\partial\theta = 0$, planar stress-displacement equations can be expressed as follows

$$\sigma_r=E(r)(c_1\frac{u_r}{r}+c_2\frac{\partial u_r}{\partial r}+\frac{c_1}{r}\frac{\partial u_\theta}{\partial \theta}), \tag{12}$$

$$\sigma_\theta=E(r)(c_1\frac{\partial u_r}{\partial r}+c_2\frac{u_r}{r}+\frac{c_2}{r}\frac{\partial u_\theta}{\partial \theta}), \tag{13}$$

$$\tau_{r\theta}=\frac{c_2-c_1}{2}E(r)(\frac{1}{r}\frac{\partial u_r}{\partial \theta}+\frac{\partial u_\theta}{\partial r}-\frac{u_\theta}{r}), \tag{14}$$

Then, by substitution of Eqs. (12) to (14) in equilibrium Eqs (3) and (4) and by carrying out differentiation, the dynamic equilibrium equations governing the displacements in radial and circumferential directions are rewritten as follows

$$\begin{aligned}&F_3(r)\frac{\partial^2 u_r}{\partial r^2}+[F_4(r)+\frac{F_3(r)}{r}]\frac{\partial u_r}{\partial r}+[\frac{F_2(r)}{r}-\frac{F_3(r)}{r^2}]u_r\\&+[\frac{F_2(r)}{r}-\frac{F_4(r)}{r^2}+\frac{F_1(r)}{2r^2}]\\&+[\frac{F_1(r)+F_3(r)}{2r}]\frac{\partial^2 u_\theta}{\partial r\partial\theta}+[\frac{F_3(r)-F_1(r)}{2r^2}]\frac{\partial^2 u_r}{\partial\theta^2}\\&+r\omega^2(t)=0,\end{aligned} \tag{15}$$

$$\begin{aligned}&[\frac{F_1(r)+F_3(r)}{2r}]\frac{\partial^2 u_r}{\partial r\partial\theta}+[\frac{F_4(r)-F_2(r)}{2r}+\frac{3F_3(r)-F_1(r)}{2r^2}]\frac{\partial u_r}{\partial\theta}\\&+\frac{F_3(r)}{r^2}\frac{\partial^2 u_\theta}{\partial\theta^2}+[\frac{F_3(r)-F_3(r)}{2}]\frac{\partial^2 u_\theta}{\partial r^2}\\&+[\frac{F_4(r)-F_2(r)}{2}+\frac{F_3(r)-F_1(r)}{2r}]\frac{\partial u_\theta}{\partial r}\\&-[\frac{F_4(r)-F_2(r)}{2r}+\frac{F_3(r)-F_1(r)}{2r^2}]u_r-r\frac{d\omega(t)}{dt}=0,\end{aligned} \tag{16}$$

in which

$$\begin{aligned}&F_1(r)=c_1\frac{E(r)}{\rho(r)},\ F_2(r)=\frac{c_1}{\rho(r)}\frac{dE(r)}{dr},\\&F_3(r)=c_2\frac{E(r)}{\rho(r)},\ F_4(r)=\frac{c_2}{\rho(r)}\frac{dE(r)}{dr},\end{aligned} \tag{17}$$

Solving the governing equations of the rotating disk

In order to resolve the equations (15) and (16), governing the radial and circumferential displacements of the disk, the method of separation of variables is applied, in which the time-dependent displacement function is defined as the multiplication of two functions $R(r)$ and $T(t)$, it means that [18, 19, and 20]

$$u_r(r,t)=R_r(r)T_r(t), \tag{18}$$

$$u_\theta(r,t)=R_\theta(r)T_\theta(t), \tag{19}$$

In this paper, it should be noted that the angular speed function governing the rotation of the disk is considered as an arbitrary function with constant value angular speed, decelerated exponential function, accelerated/decelerated linear function, accelerated quadratic function, and accelerated square root function. Without losing the generality of the solution method, this method is illustrated in an example in which an exponential function is considered for the angular speed of the disk as [18, 19, and 20]

$$\omega(t)=\omega_0 e^{-\lambda t},\ \omega,\lambda=cte., \tag{20}$$

Also, to eliminate the time variable t in the equilibrium equations of the disk (equations (15) and (16)), the equations $T_r(t)$ and $T_\theta(t)$ are considered as follows

$$T_r(t)=e^{-2\lambda t}, \tag{21}$$

$$T_\theta(t) = e^{-\lambda t}, \tag{22}$$

Now, by substituting equations (18) to (20) in the dynamic equilibrium equation governing the radial and circumferential displacement of the disk (equations (15) and (16)) and after simplifying the obtained equations, the general form of the BVP governing equations are obtained as follows [18 and 19]

$$R_r''(r) + g_1(r)R_r'(r) + g_2(r)R_r(r) = g_3(r), \tag{23}$$

$$R_\theta''(r) + g_4(r)R_\theta'(r) + g_5(r)R_\theta(r) = g_6(r), \tag{24}$$

where

$$g_1(r) = \left[\frac{F_4(r)}{F_3(r)} + \frac{1}{r}\right],\ g_2(r) = \frac{1}{r}\left[\frac{F_2(r)}{F_3(r)} - \frac{1}{r}\right],$$
$$g_3(r) = -\frac{r\omega_0^{\ 2}}{F_3(r)},\ g_4(r) = \frac{F_4(r) - F_2(r)}{F_3(r) - F_1(r)} + \frac{1}{r}, \tag{25}$$
$$g_5(r) = \frac{1}{r}\left[\frac{F_4(r) - F_2(r)}{F_1(r) - F_3(r)} - \frac{1}{r}\right],\ g_6(r) = \frac{2r\lambda\omega_0}{F_1(r) - F_3(r)},$$

It is to be noted that in Eqs. (23) and (24), prime superscripts over any parameter indicate the derivative to the radial coordinate to the same order. For solving equations (23) and (24), shooting method is used so that each of the boundary value equations (BVP) is converted to the three initial value equations (IVP) governing the functions $R_1(r)$, $R_2(r)$, and $R_0(r)$, the linear combination of the solutions of these three equations is the final solution of equations (23) and (24). So, to solve Eq. (23), we have

$$R_1''(r) + g_1(r)R_1'(r) + g_2(r)R_1(r) = 0,\quad R_1(a) = 1,\ R_1'(a) = 0, \tag{26}$$

$$R_2''(r) + g_1(r)R_2'(r) + g_2(r)R_2(r) = 0,\quad R_2(a) = 0,\ R_2'(a) = 1, \tag{27}$$

$$R_0''(r) + g_1(r)R_0'(r) + g_2(r)R_0(r) = g_3(r),\quad R_0(a) = 0,\ R_0'(a) = 0, \tag{28}$$

where the answer to Eq. (23) is as follows

$$R_r(r) = s_1R_1(r) + s_2R_2(r) + R_0(r), \tag{29}$$

It should be noted that the numerical coefficients of s_1 and s_2 are obtained from the governing boundary conditions of the rotating disk. Also, to solve Eq. (24), the following three equations are considered

$$R_1''(r) + g_4(r)R_1'(r) + g_5(r)R_1(r) = 0,\quad R_1(a) = 1,\ R_1'(a) = 0, \tag{30}$$

$$R_2''(r) + g_4(r)R_2'(r) + g_5(r)R_2(r) = 0,\quad R_2(a) = 0,\ R_2'(a) = 1, \tag{31}$$

$$R_0''(r) + g_4(r)R_0'(r) + g_5(r)R_0(r) = g_6(r),\quad R_0(a) = 0,\ R_0'(a) = 0, \tag{32}$$

The solution of Eq. (24) is obtained as a linear combination of solutions of equations (30) to (32) as follows

$$R_\theta(r) = s_3R_1(r) + s_4R_2(r) + R_0(r), \tag{33}$$

where numerical coefficients of s_3 and s_4 are obtained from the boundary conditions governing the rotating disk.

Boundary conditions governing the rotating disk

It is assumed that the displacement in the inner radius a, and the stress in the outer radius b is zero. It means

$$u_r\big|_{r=a} = 0, \sigma_r\big|_{r=b} = 0, \tag{34}$$

$$u_\theta\big|_{r=a} = 0, \sigma_\theta\big|_{r=b} = 0, \tag{35}$$

By substituting boundary conditions (Eq. (34)) in equations (12), (14), and (18), boundary conditions are achieved for Eq. (23) as follows

$$R_r(a) = 0,\ c_2R_r'(b) + \frac{c_1}{b}R_r(b) = 0, \tag{36}$$

By combining the boundary conditions (Eq. (36)) and Eq. (29), and by solving the equations with associated initial conditions numerically (equations (26) to (28)) in order to obtain the values $R_1(b)$, $R_1'(b)$, $R_2(b)$ and $R_2'(b)$, the numerical coefficients of s_1 and s_2 in Eq. (29) are calculated as follows

$$[c_2R_1'(b) + \frac{c_1}{b}R_1(b)]s_1 + [c_2R_2'(b) + \frac{c_1}{b}R_2(b)]s_2 = -c_2R_0'(b) + \frac{c_1}{b}R_0(b),\ s_1 = 0, \tag{37}$$

With this method, by applying the rotating disk boundary conditions (Eq. (25)) to equations (12), (14), and (19), the boundary conditions of Eq. (24) are defined as follows

$$R_\theta(a) = 0,\ c_2R_\theta'(b) - \frac{R_\theta(b)}{b} = 0, \tag{38}$$

By combining the boundary conditions (Eq. (33)) and Eq. (38) and by solving the equations with associated initial conditions numerically (equations (30) to (32)) in order to obtain the values $R_1(b)$, $R_1'(b)$, $R_2(b)$ and $R_2'(b)$, the

numerical coefficients of s_3 and s_4 in Eq. (33) are calculated as follows

$$[R_1'(b)-\frac{R_1(b)}{b}]s_3+[R_2'(b)-\frac{R_2(b)}{b}]s_4 = -R_0'(b)+\frac{R_0(b)}{b},\ s_3=0, \quad (39)$$

Therefore, functions R_r and R_θ, are calculated. Then, functions $u_r(r, t)$ and $u_\theta(r, t)$ in equations (18) and (19) are defined and obtained. In the following, radial stresses $\sigma_r(r, t)$, circumferential stress $\sigma_\theta(r, t)$ and shear stress $\tau_{r\theta}(r, t)$ are determined from equations (12) to (14). It should be noted that the equations governing the displacement and stress obtained through the analytical method are solved numerically using the shooting method with the help of the codes developed in the MATLAB mathematical software. Also, the finite element modeling is performed by writing a subroutine in the ANSYS software environment.

Equations governing the plastic region of the rotating disk

The von Mises criterion

The von Mises yield criterion is applied for evaluating the plastic behavior of the rotating disk. According to the assumption that the disk radius is much larger than the disk thickness ($R >> t$), for the understudied plane stress problem, the deviatoric tensor is expressed as follows [5, 19, 21, 22, 24, and 25]

$$[S_{ij}]=\begin{bmatrix}\sigma_r-\hat{\sigma} & 0\\ 0 & \sigma_\theta-\hat{\sigma}\end{bmatrix}, \quad (40)$$

$$\hat{\sigma}=[\sigma_r+\sigma_\theta]/3, \quad (41)$$

where $\hat{\sigma}$ is hydrostatic stress. The yield criterion of the von Mises is written as an indicial form equation in terms of the deviatoric stress tensor as follows

$$\sigma_{eq}=\sqrt{\frac{3}{2}S_{ij}S_{ji}}, \quad (42)$$

By substituting Eq. (40) in Eq. (42), the von Mises yield criterion is rewritten as

$$\sigma_{eq}=\sqrt{(3/2)(\sigma_r-\hat{\sigma})(\sigma_\theta-\hat{\sigma})}= \sqrt{(3/2)[\sigma_r-(\sigma_r+\sigma_\theta)/3][\sigma_\theta-(\sigma_r+\sigma_\theta)/3]} = \sqrt{\sigma_r^2+\sigma_\theta^2-\sigma_r\sigma_\theta}, \quad (43)$$

The Prandtl-Reuss equation

The Prandtl-Reuss equation is stated as follows [5, 19, 21, 22, 24, and 25]

$$d\varepsilon_{ij}^p=S_{ij}d\lambda, \quad (44)$$

where $d\lambda$ is a non-negative scalar quantity. Using the above equation, the equations governing the change of plastic strain $d\varepsilon_{ij}^p$, along the radial direction ($d\varepsilon_r^p$), circumferential direction ($d\varepsilon_\theta^p$) and along the thickness ($d\varepsilon_z{}^p$) of the rotating disk are expressed, respectively, as follows

$$d\varepsilon_r^p=\frac{2}{3}d\lambda(\sigma_r-\frac{\sigma_\theta}{2})=\frac{1}{3}d\lambda(2\sigma_r-\sigma_\theta), \quad (45)$$

$$d\varepsilon_\theta^p=\frac{2}{3}d\lambda(\sigma_\theta-\frac{\sigma_r}{2})=\frac{1}{3}d\lambda(2\sigma_\theta-\sigma_r), \quad (46)$$

$$d\varepsilon_z^p=\frac{2}{3}d\lambda[-\frac{1}{2}(\sigma_r+\sigma_\theta)]=-\frac{1}{3}d\lambda(\sigma_r+\sigma_\theta), \quad (47)$$

And the differentiation of the equivalent plastic strain $d\varepsilon_{eq}$, in terms of the strain differentiation in three directions, is stated as follows

$$d\varepsilon_{eq}=\sqrt{2/3}\sqrt{d\varepsilon_{ij}^p.d\varepsilon_{ji}^p} =\sqrt{2/3}\sqrt{(d\varepsilon_r^p)^2+(d\varepsilon_\theta^p)^2+(d\varepsilon_z^p)^2}, \quad (48)$$

From the substitution of equations (45) to (47) in Eq. (48), and also due to the non-variable nature of the volume in plastic strain mode (i.e., $d\varepsilon_r^p+d\varepsilon_\theta^p+d\varepsilon_z^p=0$), the quantity $d\lambda$ is calculated as follows

$$\begin{aligned}d\varepsilon_{eq}&=\{\frac{2}{3}([\frac{1}{3}d\lambda(2\sigma_r-\sigma_\theta)]^2+[\frac{1}{3}d\lambda(2\sigma_\theta-\sigma_r)]^2\\&\quad+[-\frac{1}{3}d\lambda(\sigma_r+\sigma_\theta)]^2\}^{1/2}\\&=\{\frac{2}{3}[\frac{1}{9}d\lambda^2(4\sigma_r^2+\sigma_\theta^2-4\sigma_r\sigma_\theta+4\sigma_\theta+\sigma_r^2\\&\quad-4\sigma_r\sigma_\theta+\sigma_r^2+\sigma_\theta^2+2\sigma_r\sigma_\theta)]\}^{1/2}\\&=[\frac{2}{27}d\lambda^2(6\sigma_r^2+6\sigma_\theta^2-6\sigma_r\sigma_\theta)]^{1/2}\Rightarrow d\lambda=\frac{3}{2}\frac{d\varepsilon_{eq}}{\sigma_y},\end{aligned} \quad (49)$$

By substituting value obtained for $d\lambda$ from Eq. (49) in equations (45) to (47), the terms relating to the plastic strain differentiation in three directions are rewritten as follows [5, 19, 21, 22, 24, and 25]

$$\varepsilon_r^p=\frac{\varepsilon_{eq}}{\sigma_y}(\sigma_r-\frac{1}{2}\sigma_\theta), \quad (50)$$

$$\varepsilon_\theta^p=\frac{\varepsilon_{eq}}{\sigma_y}(\sigma_\theta-\frac{1}{2}\sigma_r), \quad (51)$$

$$\varepsilon_z^p=\frac{\varepsilon_{eq}}{\sigma_y}(\sigma_r+\sigma_\theta), \quad (52)$$

Equation of Ludwig hardening law

The relation between stress and strain using the Ludwig equation is

$$\sigma = \sigma_y + H\varepsilon^n, \tag{53}$$

where H is the strain hardening rate, σ_y is the yielding stress of material, and n is the material-dependent parameter. The relationship between the yield stress and the equivalent plastic strain is expressed as [5, 19, 21, 22, 24, and 25]

$$\varepsilon_{eq} = (\frac{\sigma_{eq} - \sigma_y}{H})^{1/n}, \tag{54}$$

By substituting Eq. (54) in plastic strain equations (50) and (51), it is obtained that

$$\varepsilon_r^p = \frac{1}{\sigma_{eq} H^{1/n}} (\sigma_{eq} - \sigma_y)^{1/n} (\sigma_r - \frac{\sigma_\theta}{2}), \tag{55}$$

$$\varepsilon_\theta^p = \frac{1}{\sigma_{eq} H^{1/n}} (\sigma_{eq} - \sigma_y)^{1/n} (\sigma_\theta - \frac{\sigma_r}{2}), \tag{56}$$

Also, the elastic strain in the radial and circumferential directions are stated as

$$\varepsilon_r^e = \frac{1}{E}(\sigma_r - \nu\sigma_\theta), \tag{57}$$

$$\varepsilon_\theta^e = \frac{1}{E}(\sigma_\theta - \nu\sigma_r), \tag{58}$$

The total strain ε_{tot}, which is the sum of the elastic strains ε^e and the plastic strains ε^p are defined as follows

$$\varepsilon_{tot} = \varepsilon^p + \varepsilon^e, \tag{59}$$

Consequently, the sum of elastic and plastic strains in the radial and circumferential directions is obtained as follows [5, 19, 21, 22, 24, and 25]

$$\varepsilon_r = \frac{1}{\sigma_{eq} H^{1/n}} (\sigma_{eq} - \sigma_y)^{1/n} (\sigma_r - \frac{\sigma_\theta}{2}) + \frac{1}{E}(\sigma_r - \nu\sigma_\theta), \tag{60}$$

$$\varepsilon_\theta = \frac{1}{\sigma_{eq} H^{1/n}} (\sigma_{eq} - \sigma_y)^{1/n} (\sigma_\theta - \frac{\sigma_r}{2}) + \frac{1}{E}(\sigma_\theta - \nu\sigma_r), \tag{61}$$

Equation governing the hardening behavior of the rotating disk in the plastic region

According to equations (5) and (6) in the axisymmetric condition, the strain-displacement equations are defined as follows

$$\varepsilon_r = \frac{du_r}{dr}, \tag{62}$$

$$\varepsilon_\theta = \frac{u_r}{r}, \tag{63}$$

In other words, from equations (62) and (63), we have

$$\varepsilon_r = \varepsilon_\theta + r\frac{d\varepsilon_\theta}{dr}, \tag{64}$$

The following equation is obtained by substituting the plastic strain equations (60) and (61) in strain-displacement equation (64)

$$\begin{aligned} &\frac{1}{\sigma_{eq} H^{1/n}} (\sigma_{eq} - \sigma_y)^{1/n} (\sigma_r - \sigma_\theta) + \frac{1}{E(r)}(\sigma_r - \nu\sigma_\theta) \\ &= \frac{1}{\sigma_{eq} H^{1/n}} (\sigma_{eq} - \sigma_y)^{1/n} (\sigma_\theta - \frac{\sigma_r}{2}) + \frac{1}{E(r)}(\sigma_\theta - \nu\sigma_r) \\ &+ r\frac{d}{dr}[\frac{1}{\sigma_{eq} H^{1/n}} (\sigma_{eq} - \sigma_y)^{1/n} (\sigma_\theta - \frac{\sigma_r}{2}) + \frac{1}{E(r)}(\sigma_\theta - \nu\sigma_r)], \end{aligned} \tag{65}$$

The following equation is obtained by differentiation from the right-hand term in Eq. (65) and simplifying the expression on the left hand side, as well as the replacement of m=1/n in it.

$$\begin{aligned} &\frac{d\varepsilon_\theta}{dr} = \frac{m}{\sigma_{eq}^2 H^{2m}} (\sigma_{eq} - \sigma_y)^{m-1} \sigma_{eq} H^m (\frac{d\sigma_{eq}}{dr} - \frac{d\sigma_r}{dr})(\sigma_\theta - \frac{\sigma_r}{r}) \\ &-[\frac{1}{\sigma_{eq}^2 H^{2m}} (\sigma_{eq} - \sigma_y)^m] H^m (\sigma_\theta - \frac{\sigma_r}{r}) \\ &+ (\frac{d\sigma_\theta}{dr} - \frac{1}{2}\frac{d\sigma_r}{dr}) \frac{1}{\sigma_{eq} H^m} (\sigma_{eq} - \sigma_y)^m \\ &+ \frac{1}{E(r)}(\frac{d\sigma_\theta}{dr} - \nu\frac{d\sigma_r}{dr}) - \frac{1}{E(r)^2}\frac{dE(r)}{dr}(\sigma_\theta - \nu\sigma_r), \end{aligned} \tag{66}$$

$$\varepsilon_r - \varepsilon_\theta = \frac{3(1+\nu)}{2E(r)} \frac{1}{r\sigma_{eq}^2 H^{2m}} (\sigma_{eq} - \sigma_y)^m (\sigma_r - \sigma_\theta), \tag{67}$$

To simplify by defining the following parameters

$$\begin{aligned} &Z = \sigma_{eq} H^m (\sigma_{eq} - \sigma_y)^{m-1}, T = \frac{(\sigma_{eq} - \sigma_y)^m}{\sigma_{eq} H^m}, \\ &D = \frac{mZ}{\sigma_{eq}^2 H^{2m}} (\sigma_\theta - \frac{\sigma_r}{2}), P = \frac{H^m (\sigma_{eq} - \sigma_y)^m}{\sigma_{eq}^2 H^{2m}} (\sigma_\theta - \frac{\sigma_r}{2}), \\ &G = \frac{3(1+\nu)(\sigma_{eq} - \sigma_y)^m}{2E(r)\sigma_{eq}^2 H^{2m}}, \end{aligned} \tag{68}$$

The equations (66) and (67) are rewritten as follows

$$\begin{aligned} &\frac{d\varepsilon_\theta}{dr} = D(\frac{d\sigma_{eq}}{dr} - \frac{d\sigma_y}{dr}) - P\frac{d\sigma_{eq}}{dr} + T(\frac{d\sigma_\theta}{dr} - \frac{1}{2}\frac{d\sigma_r}{dr}) \\ &+ \frac{1}{E(r)}(\frac{d\sigma_\theta}{dr} - \nu\frac{d\sigma_r}{dr}) - \frac{1}{E(r)^2}\frac{dE(r)}{dr}(\sigma_\theta - \nu\sigma_r), \end{aligned} \tag{69}$$

$$\frac{\varepsilon_r - \varepsilon_\theta}{r} = \frac{G(r)}{r}(\sigma_r - \sigma_\theta), \tag{70}$$

By substituting the equations (69) and (70) in Equation (64)

$$\begin{aligned} &(D-P)\frac{d\sigma_{eq}}{dr} - D\frac{d\sigma_y}{dr} + (T + \frac{1}{E(r)})\frac{d\sigma_\theta}{dr} - (\frac{T}{2} + \nu)\frac{d\sigma_r}{dr} \\ &- \frac{1}{E(r)^2}\frac{dE(r)}{E(r)}(\sigma_\theta - \nu\sigma_r) - \frac{G(r)}{r}(\sigma_r - \sigma_\theta) = 0, \end{aligned} \tag{71}$$

which we have in equation (71)

$$\begin{aligned} &\frac{d\sigma_{eq}}{dr} = (\frac{2\sigma_r - \sigma_\theta}{2\sigma_{eq}})\frac{d\sigma_r}{dr} + (\frac{2\sigma_\theta - \sigma_r}{2\sigma_{eq}})\frac{d\sigma_\theta}{dr}, \\ &\sigma_r = \frac{Y}{r}, \frac{d\sigma_r}{dr} = \frac{dY/dr}{r} - \frac{Y}{r^2}, \sigma_\theta = dY/dr + \rho r^2\omega^2, \\ &\frac{d\sigma_\theta}{dr} = d^2Y/dr^2 + \frac{d\rho}{dr}r^2\omega^2 + 2r\rho\omega^2, \end{aligned} \tag{72}$$

In equation (72), Y is the yield stress function. By substituting the above equations in Eq. (65), the final equation governing the behavior of the disk in the plastic region is obtained as follows

$$\begin{aligned}&[(mN_4-H^mN_5)(\sigma_\theta-\sigma_r/2)\frac{N_2}{2\sigma_{eq}}+N_6+1/E]\frac{d^2Y}{dr^2}\\&+\{(mN_4-H^mN_5)(\sigma_\theta-\sigma_r/2)\frac{N_1}{2\sigma_{eq}}[2r\rho(r)\omega^2+r^2\omega^2\frac{d\rho(r)}{dr}]\}\\&-\frac{d\sigma_y}{dr}+2r\rho(r)\omega^2N_6+r^2\omega^2\frac{d\rho(r)}{dr}N_6+\frac{1}{2}\frac{d\sigma_r}{dr}+\frac{2\rho(r)r\omega^2}{E}\\&+\frac{r^2\omega^2\frac{d\rho(r)}{dr}}{E}-\nu\frac{d\sigma_r}{dr}-(\frac{3}{2}N_6+\frac{1+\nu}{E})(\sigma_r-\sigma_\theta)=0,\end{aligned} \quad (73)$$

where

$$\begin{aligned}&N_1=(2\sigma_r-\sigma_\theta)\frac{d\sigma_r}{dr},\ N_2=(2\sigma_\theta-\sigma_r),\\&N_3=2r\rho(r)\omega^2+r^2\omega^2\frac{d\rho(r)}{dr},\\&N_4=(\sigma_{eq}-\sigma_y)^{m-1}\sigma_{eq}H^m,\\&N_5=(\sigma_{eq}-\sigma_y)^m,\ N_6=[\frac{(\sigma_{eq}-\sigma_y)^m}{\sigma_{eq}H^m}],\end{aligned} \quad (74)$$

It is to be mentioned that the equation governing the stresses in the plastic region in the analytical method is solved with the help of developed codes in the MATLAB mathematical programming environment.

Evaluating the results from the analytical and numerical methods

In this section, we first compared the obtained elastic and elasto-plastic results with the results reported in other references for special cases. Then, the results of analytical and numerical methods in elastic and elasto-plastic analyses for the distribution of radial displacement and radial, circumferential, and shear stresses are studied by considering the angular speed in the form of constant value, exponential, linear accelerated/decelerated, quadratic, and square root functions with varying physical and geometric properties of the rotating disk. In the following, the results of the plastic deformation analysis are presented for the FGM rotating disk. It is to be mentioned that using ANSYS software for finite element analysis, the FGM disk is modeled and meshed by Plane42 2-D structural solid axisymmetric element.

Elastic analysis results

In this section, first, the results of the elastic analysis are validated through comparing to the results available in the literature. Then, the results of elastic analysis of the rotating disk are presented by considering different functions for the rotating speed.

Validation of results

For ease of comparison and validation of the results, the geometric and mechanical specifications of the FGM rotating disk are considered according to the reference [18] (with the properties of *SUS*304 material for the metal and the properties of *Si*3*N*4 material for the ceramic).

$$a=0.02\,m,\ b=0.1\,m,\ \nu=0.3,\ \omega=100\ rad/s,$$

$$n=50,\ \rho(r)=(8166-2370)(\frac{r-0.02}{0.1-0.02})^n+2370\ kg/m^3,$$

$$E(r)=(201.04-384.43)\times10^9\times(\frac{r-0.02}{0.1-0.02})^n+348.43\times10^9\ Pa,$$

$$\sigma_y=(240-375)\times10^6\times(\frac{r-0.02}{0.1-0.02})^n+375\times10^6\ Pa,$$

In Fig. 2, the variation of elastic modulus function $E(r)$ are indicated in terms of the radial distance of the disk for different power indices of the FG material, i.e. n, (with the properties of *SUS*304 material for the metal and the properties of *Si*3*N*4 material for the ceramic) [18].

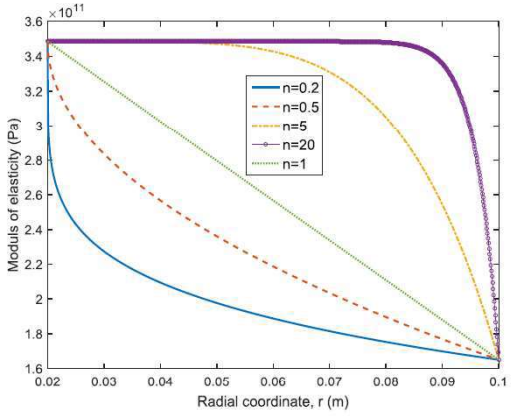

Fig. 2: The variation modulus of elasticity $E(r)$ against the radial distance of the disk for different power indices n for FG material (metal: *SUS*304 and ceramic: *Si*3*N*4)

In Fig. 3a, the radial displacement diagram is shown in terms of radial distance using the analytical and numerical solution (finite element analysis) performed in this study. In Fig. 3b, the radial displacement distribution in the disk is shown using the finite element method. In Fig. 3, it can be seen that by increasing the radial distance, the radial displacement of the disk increases from zero at the inner radius and reaches its maximum

value at the outer radius. The results show the agreement of two analytical and numerical methods used in the present study and with the trend of variation of results presented in reference [18]. In Fig. 3, the results presented by the reference [18] are also presented for comparison. It is to be noted that the results reported in [18] have lower values compared to the results of the present study. However, the trend of variation of the results shown in Fig. 3 in this paper is in consistent with the trend of variation of results reported in [18]. Moreover, the similar results reported in [18] are depicted in Figs. 4 and 5 for comparing to this study here.

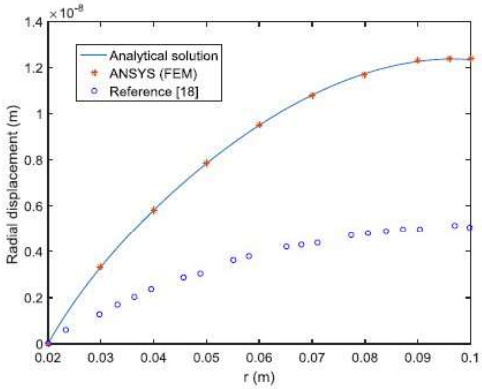

(a)

(b)

Fig. 3: a- Variation of the radial displacement in terms of the radial distance and comparison with the results of reference [18], b- 2D distribution of radial displacement in the disk using FEM

The radial stress diagram obtained from the analytical and numerical methods in this study is presented in Fig. 4. According to Fig. 4a, the results obtained from the numerical and analytical methods are in a good agreement. Also, it is seen that by increasing the radial distance, radial stresses are reduced from the maximum value at the inner radius to zero at the outer radius. In Fig. 4b the radial stress distribution in the disk is shown using the finite element method. The results show the full agreement of two analytical and numerical solution methods used in the present study and with those of the trend of variation of reference [18].

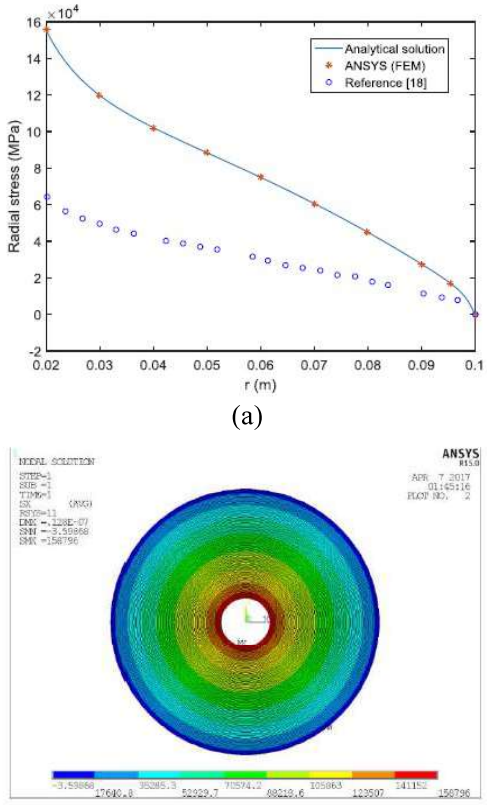

(a)

(b)

Fig. 4: a- Variation of the radial stress in terms of the radial distance and comparison with the results of reference [18], b- 2D distribution of radial stress in the disk using FEM

The results of circumferential stress diagram from the analytical and numerical methods applied in this study and reference [18] is shown in Fig. 5a. Again, as can be seen, there is a full agreement between the results obtained from analytical and numerical methods in the present study and with the trend of variation of results of reference [18]. It is observed that by increasing radial distance, the value of circumferential stress is increased to a certain radius of about 0.04 *m* and then decreases up to the ones of outer radius. Fig. 5b shows the distribution of circumferential stress in the disk obtained using the finite element method.

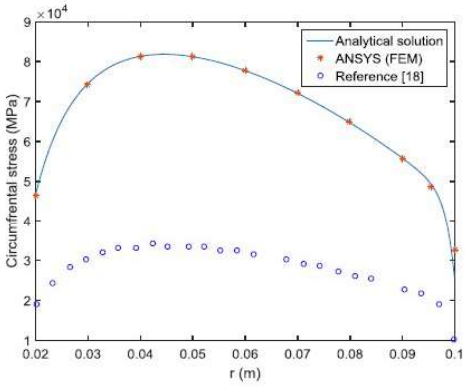

(a)

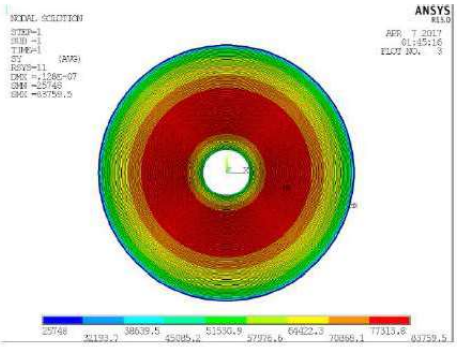

(b)

Fig. 5: a- Variation of the circumferential stress in terms of the radial distance and comparison with the results of reference [18], b- 2D distribution of radial stress in the disk using FEM

In order to validate the analytical and numerical methods presented in this paper and to compare the results with other references and to justify the accuracy of the results in elastic analysis, the following data was used [8]

$$E(r)=E_0[1-n(r/b)^k], E_0=201.04\ GPa, n=-0.6, k=1.1,$$
$$\rho=8166\ kg/m^3, a=0,\ b=1m, \nu=0.3, \omega=1000\ rpm,$$

Then, the mathematical code provided in the environment of MATLAB was run and the results obtained for normalized displacement in radial direction $\bar{u}_r$ and normalized stresses $\bar{\sigma}_r$ and $\bar{\sigma}_\theta$ in the normalized radial position $(r\text{-}a)/(b\text{-}a) = 0.5$ are 0.27, 0.7 and 0.86, respectively. The results of our method show no difference compared to the analytical solutions of Eraslan and Akis [8].

The shear stress diagram resulting from the analytical method carried out in this study is shown in Fig. 6. As observed from this graph, the shear stress decreases with the increasing radius, so that the maximum shear stress at the inner radius reaches a value of zero at the outer radius.

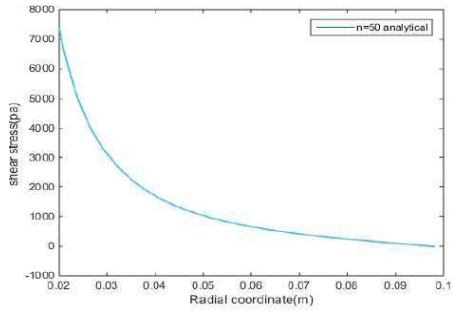

Fig. 6: Variation of the disk shear stress in terms of radial distance obtained using the analytical method

The stress and displacement diagrams of the disk with constant rotational speed

In Fig. 7, the radial displacement diagram of a rotating disk that corresponds to a constant rotational speed (ω = 100 rad/s) is shown for different values of exponent n = 0.2, 0.5, 1, 5, 10, 20, 50 applied for the properties of functionally graded material using the analytical method. From Fig. 7, it is observed that the radial displacement increases by increasing the radial distance. Also, by increasing the exponent value of functionally graded material n, the radial displacement decreases for the same radius of the disk.

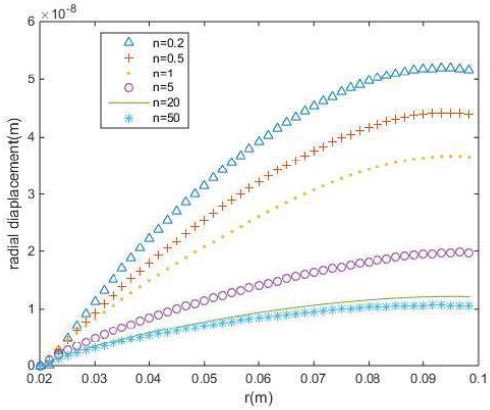

Fig. 7: Variation of the radial displacement in terms of radial distance for different values of n at constant rotating velocity ω = 100 rad/s using the analytical method

In Fig. 8, the radial stress diagram for the rotating disk that rotates with constant rotating speed of ω = 100 rad/s, is shown using the analytical method, for different values of the exponent index of functionally graded material n = 0.2, 0.5, 1, 5, 10, 20, 50. From Fig. 8, it can be seen that the radial stress is reduced from the maximum value at the

inner radius and reaches zero at the outer radius. Also, by increasing the exponent n, radial stress decreases for the same radius of the disk.

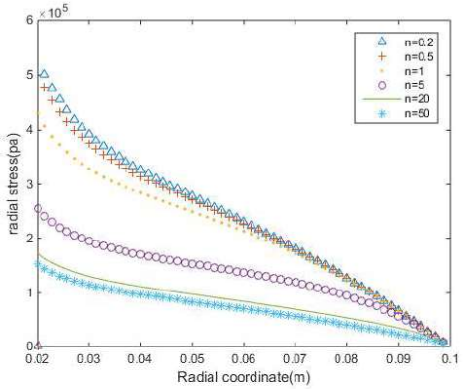

Fig. 8: Variation of the radial stress in terms of radial distance for different values of n at constant rotational speed ω = 100 rad/s using the analytical method

In Fig. 9, the circumferential stress diagram in the disk that rotates with constant rotational speed of ω =100 rad/s, is shown using the analytical method for different values of functionally graded material index n = 0.2, 0.5, 1, 5, 10, 20, 50. It is observed that by increasing the radial distance, the circumferential stress increases in the radial direction to a specific radius, and then decreases to minimum value at its outer radius. Also, by increasing the value of n, the circumferential stress is reduced for the same radius of the disk. These obtained results are in perfect agreement with the results reported in reference [18].

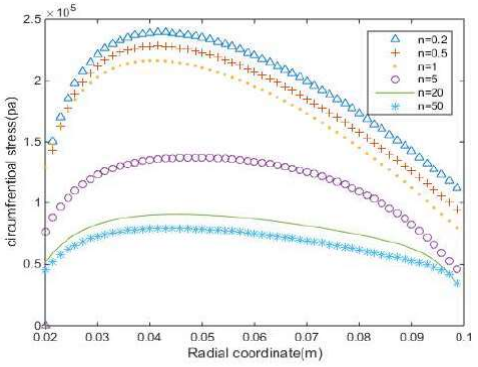

Fig. 9: Variation of the circumferential displacement in terms of radial distance for different values of n at constant rotating speed ω = 100 rad/s using the analytical method

The stress and displacement diagrams of the disk with the variable rotating speed in form of exponential function

In Fig. 10, the variation of rotating speed is shown in form of exponential function $\omega(t) = 100\,e^{-0.5t}\ rad/s$ [18], in which the rotating velocity of the disk decreases with a decelerated acceleration from the rotational speed of ω = 100 rad/s to the rotating speed of ω = 10 rad/s during a 5s period.

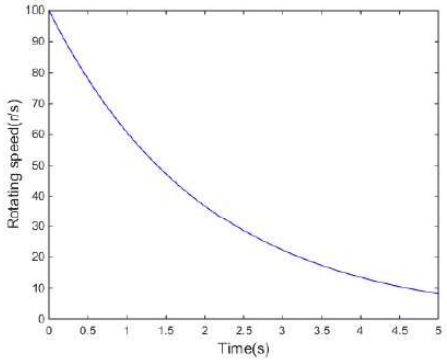

Fig. 10: Variation of rotating speed of the disk as a time-dependent exponential function

In Figs. 11, 12, 13, and 14, respectively, the three-dimensional variation of radial displacement, radial stress, circumferential stress, and shear stress are shown in terms of radial displacement and time and considering an exponential function for the rotating speed $\omega(t) = 100\,e^{-0.5t}\ rad/s$ for FGM exponent of n =1 using the analytical method.

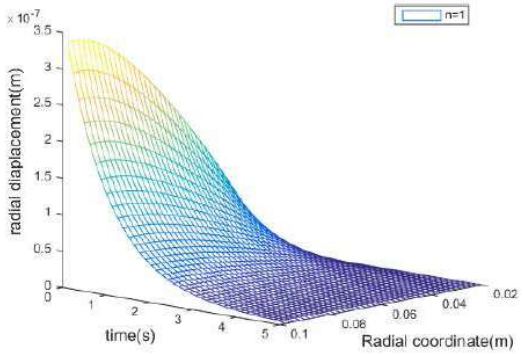

Fig. 11: The 3 D profile of radial displacement variation in terms of radial distance and time for n = 1 and considering the exponentially variable rotating speed

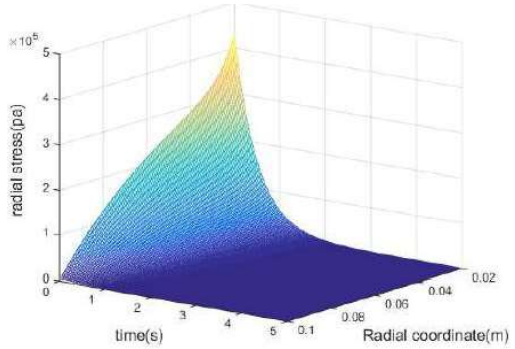

Fig. 12: The 3 D profile of radial stress variation in terms of radial distance and time for n=1 and considering the exponentially variable rotating speed

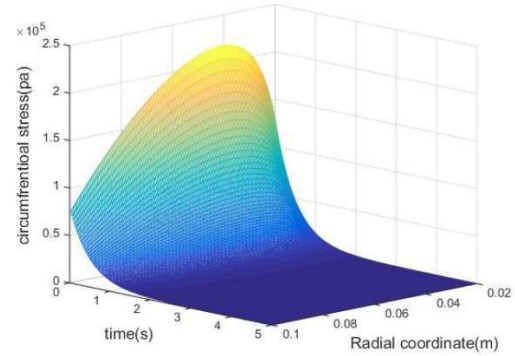

Fig. 13: The 3 D profile of circumferential stress variation in terms of radial distance and time for n = 1 and considering the exponentially variable rotating speed

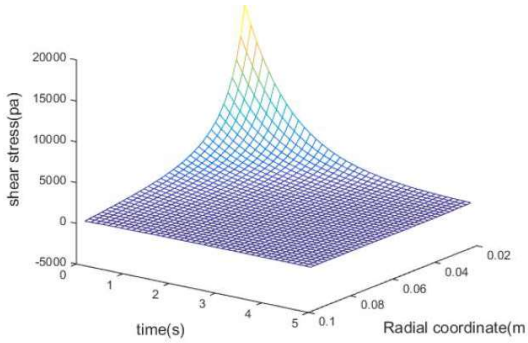

Fig. 14: The 3 D profile of shear stress variation in terms of radial distance and time for n = 1 and considering the exponentially variable rotating speed

The effects of disk geometry on mechanical behavior of the rotating disk

In this section, the effects of disk geometry on mechanical behavior of the disk of rotating speed $\omega = 100\ rad/s$ and power distribution index n =1 is investigated. The outer and inner radius of the disk are considered to be fixed with the value of b = 0.1 m and variable with the values of a = 0.02, 0.04, and 0.06 m, respectively.

In Fig. 15, the variation of radial displacement for the disk of outer radius b = 0.1 m and inner radius a = 0.02, 0.04, and 0.06 m with constant exponential rotating speed is shown for index of functionally graded material n = 1 using the analytical method. It is observed that by increasing the value of inner radius of the disk, radial displacement values are reduced along the disk radius so that the value of radial displacement in the outer radius decreases by increasing the inner radius of the disk. Also, the values of radial displacement for the disk with the inner radius a = 0.02 m are greater than that of the disk with radius a = 0.04 m and a = 0.06 m.

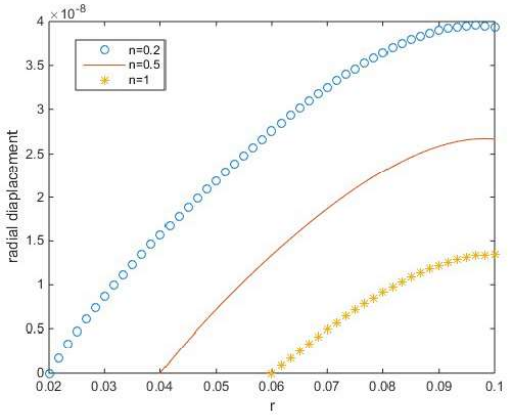

Fig. 15: Radial displacement variation for different geometries of the rotating disk with n =1 and exponential rotating speed using analytical method

In Fig. 16, the variation of radial stress for the disk of outer radius b = 0.1 m and inner radius a = 0.02, 0.04, and 0.06 m with constant rotating speed is shown for index of functionally graded material n = 1 using the analytical method. The radial stress is reduced by increasing the radial distance so that for every arbitrary inner radius of disk, the radial stress decreases from the maximum value at the inner radius of the disk to zero at the outer radius. Also, the value of radial stresses at inner radius of 0.06-0.1 m is often located on each other.

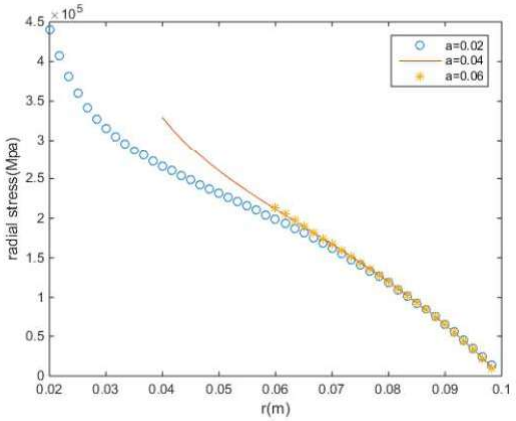

Fig. 16: The radial stress variation for different geometries of the rotating disk with n = 1 and exponential rotating velocity using the analytical method

In Fig. 17, the variation of circumferential stress for the disk of outer radius b = 0.1 m and inner radius a = 0.02, 0.04, and 0.06 m with constant rotating speed is shown for index of functionally graded material n = 1 using the analytical method. It is observed that the value of circumferential stress increases by increasing the radial distance to a specified value and then it is reduced so that it reaches the minimum value at the outer radius. The results show that the value of circumferential stress for the disk with the inner radius a = 0.02 m is greater than that of the disk with inner radius a = 0.04 m and a =0.06 m.

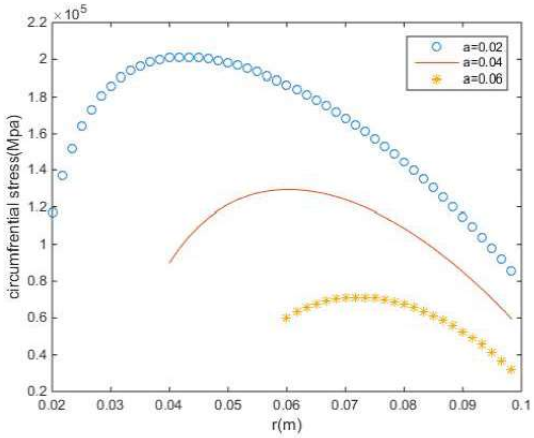

Fig. 17: The circumferential stress variation for different geometries of the rotating disk with n = 1 and exponential rotating velocity using the analytical method

It should be noted that the results of variation of parameters obtained in the present study (Figs. 6-17) are in a proper and good agreement with the reported results of reference [18]. Thus, according to validation of results, the authors ensure that the computer codes developed based on the analytical method and conducted simulations based on the finite element method have good accuracy and reliability.

Elastic analysis of the rotating annular thin disk considering different accelerated/decelerated rotating speeds

The displacement and stress diagrams of the disk with an accelerated linear rotational speed

In Fig. 18, the variation of the time function of accelerated linear rotating speed $\omega = 18t + 10\ rad/s$ is shown in which the rotating speed of the disk increases with a linear acceleration from ω = 10 rad/s to ω = 100 rad/s in a 5s period.

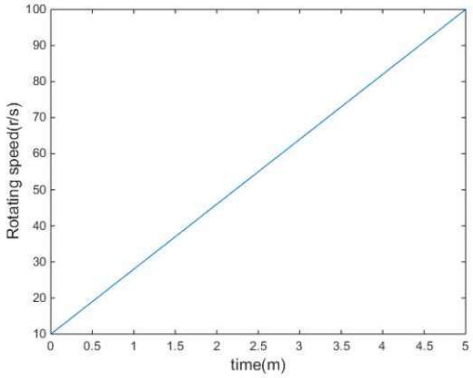

Fig. 18: Variation of the linear accelerated rotating speed of the disk with an accelerated linear trend

In Figs. 19a and 19b, the radial stress diagram of the rotating disk with an accelerated linear rotating speed for different values of FGM index n = 0.2, 0.5, 1, 5, 20, 50 is shown using the analytical method at the third and the fifth seconds, respectively. From Fig. 19, it is observed that the radial stress in the radial direction decreases from the maximum value at the inner radius to zero at the outer radius as the radial distance increases in the disk. Also, by increasing n, the radial stress decreases for the same radius of the disk.

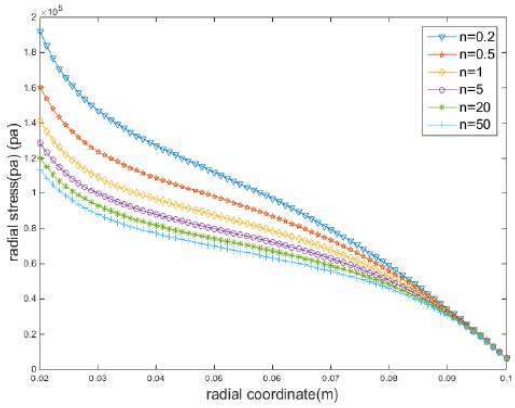

(a)

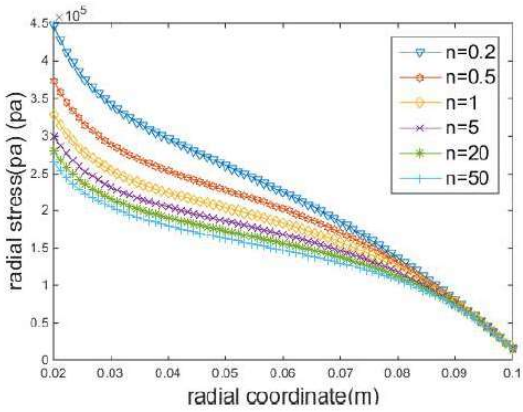

(b)

Fig. 19: Variation of the radial stress in terms of radial distance for different values of n at an accelerated linear rotating speed $\omega = 18t + 10\ rad/s$ using the analytical method, (a)- the third second and (b)- the fifth second

In Figs. 20a and 20b, the circumferential stress diagram of the rotating disk with an accelerated linear rotating speed for different values of FGM index n = 0.2, 0.5, 1, 5, 20, 50 is shown using the analytical method at the third and the fifth seconds, respectively. From Fig. 19, it is observed that by increasing the radial distance, the circumferential stress in the radial direction increases up to radius of 0.04 m and then decreases accordingly. Also, by increasing n, the circumferential stress decreases for the same radius of the disk.

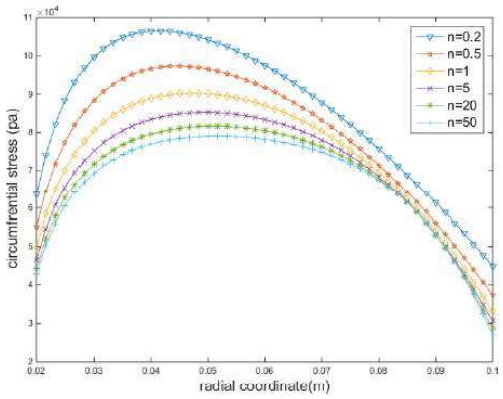

(a)

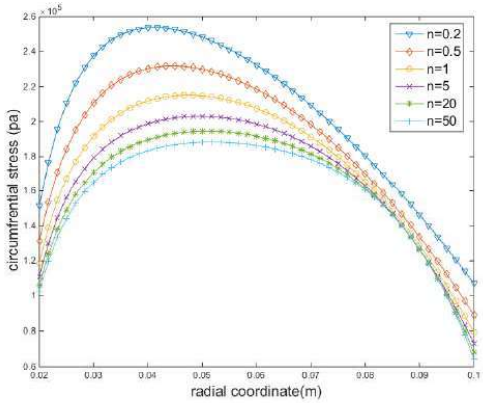

(b)

Fig. 20: Variation of the circumferential stress in terms of radial distance for different values of n at an accelerated linear rotating speed $\omega = 18t + 10\ rad/s$ using the analytical method, (a)- the third second and (b)- the fifth second

In Figs. 21a and 21b, the shear stress diagram of the rotating disk with an accelerated linear rotating speed for different values of FGM index n = 0.2, 0.5, 1, 5, 20, 50 is shown using the analytical method at the third and the fifth seconds, respectively. As can be seen the shear stress in the radial direction decreases from the maximum value at the inner radius to zero at the outer radius by increasing the radial distance in the disk.

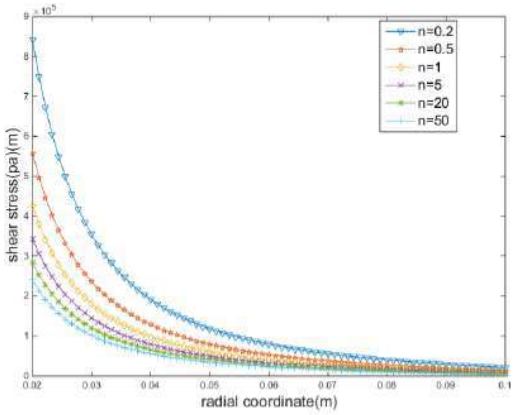

(a)

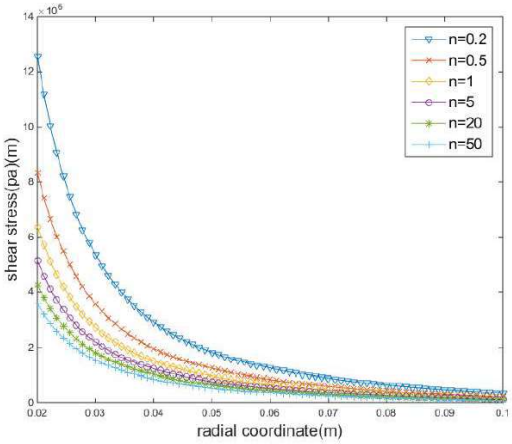

(b)

Fig. 21: Variation of the shear stress in terms of radial distance for different values of n at an accelerated linear rotating speed $\omega = 18t + 10\ rad/s$ using the analytical method, (a)- the third second and (b)- the fifth second

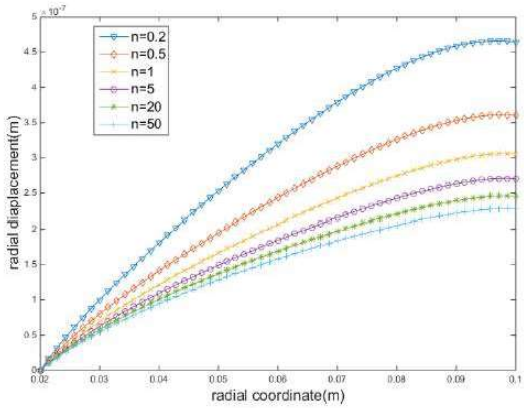

(a)

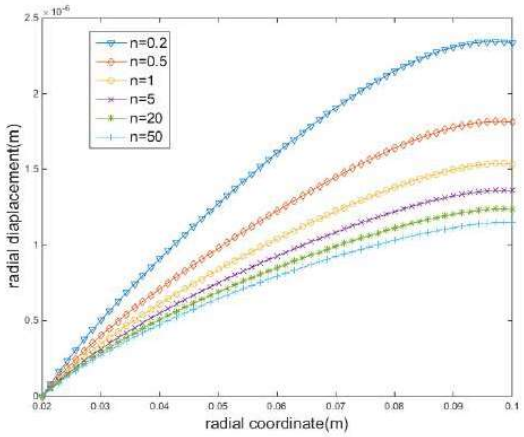

(b)

Fig. 22: Variation of the radial displacement in terms of radial distance for different values of n at an accelerated linear rotating speed $\omega = 18t + 10\ rad/s$ using the analytical method, (a)- the third second and (b)- the fifth second

In Figs. 22a and 22b, the radial displacement diagram of the rotating disk with an accelerated linear rotating speed for different values of FGM index n = 0.2, 0.5, 1, 5, 20, 50 is shown using the analytical method at the third and the fifth seconds, respectively. From Fig. 22, it is observed that the radial displacement increases by increasing the radial distance. Also, by increasing n, the radial displacement decreases for the same radius of the disk.

In Figs. 23, 24, 25, and 26, respectively, the three-dimensional model of variation for radial displacement, radial stress, circumferential stress, and shear stress are shown in terms of time and radial distance and considering the accelerated function of $\omega = 18t + 10\ rad/s$ for the rotating speed of the disk and for given value of FGM power index n using the analytical method.

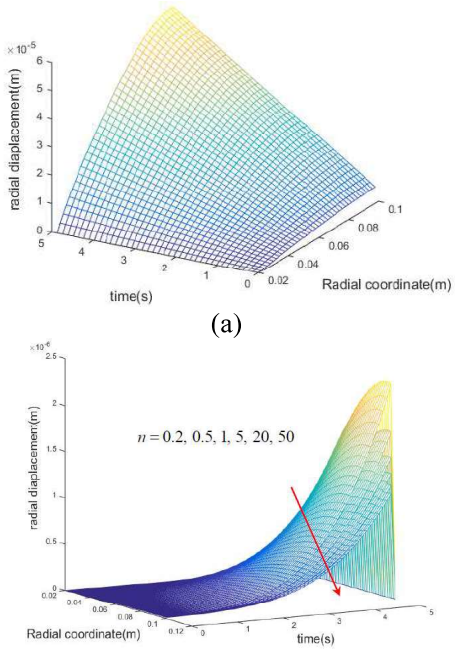

Fig. 23: Three-dimensional profile of radial displacement variation in terms of radial distance and time increase with an accelerated linear rotating speed (a)- for n = 1, (b)- for different values of n

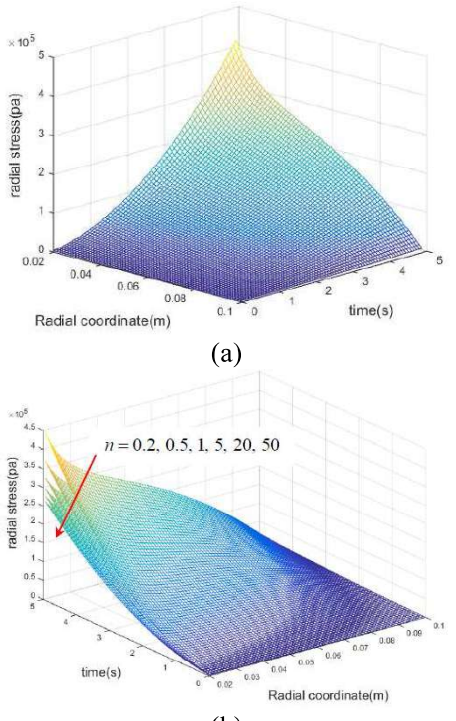

Fig. 24: Three-dimensional profile of radial stress variation in terms of radial distance and time increase with an accelerated linear rotating speed (a)- for n = 1, (b)- for different values of n

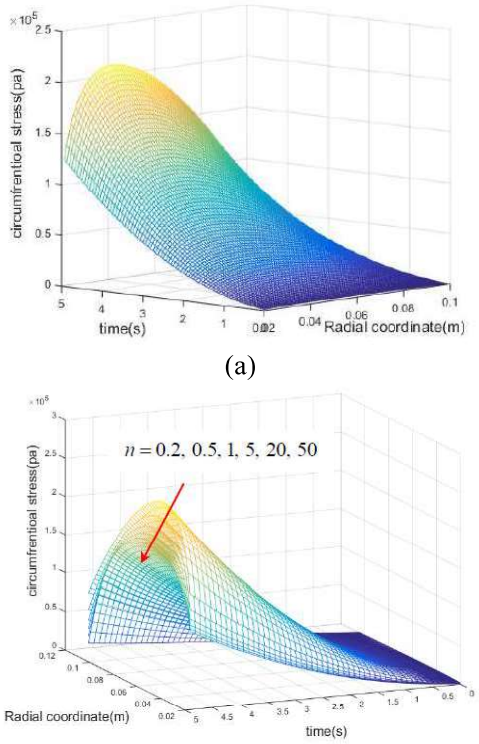

Fig. 25: Three-dimensional profile of circumferential stress variation in terms of radial distance and time increase with an accelerated linear rotating speed (a)- for n = 1, (b)- for different values of n

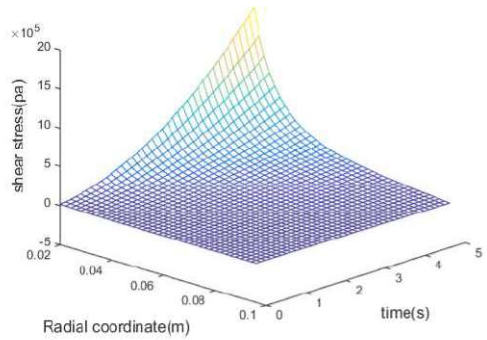

Fig. 26: The 3D profile of shear stress variation in terms of radial distance and time increase for n = 1 with the accelerated linear rotating speed

The displacement and stress diagrams of the disk with a decelerated linear rotational speed

In Fig. 27, the variation of the time function of decelerated linear rotating speed $\omega = -18t + 100\ rad/s$ is shown in which the rotating speed of the disk decreases with a linear deceleration from ω = 100 rad/s to ω = 10 rad/s in a 5 s period of time.

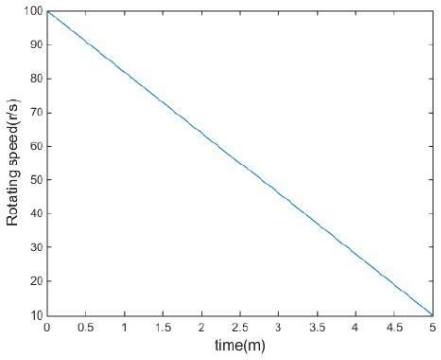

Fig. 27: Variation of the rotating speed of the disk with a decelerated linear trend

In Figs. 28, 29, 30, and 31, respectively, the three-dimensional profile of variation for radial displacement, radial stress, circumferential stress, and shear stress are shown in terms of time increase and considering the accelerated function of $\omega = -18t + 100\ rad/s$ for the rotating speed of the disk and for given value of FGM power index n using the analytical method.

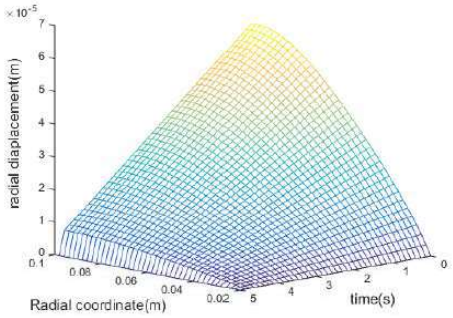

Fig. 28: Three-dimensional profile of radial displacement variation in terms of radial distance and time increase with a decelerated linear rotating speed for n = 1

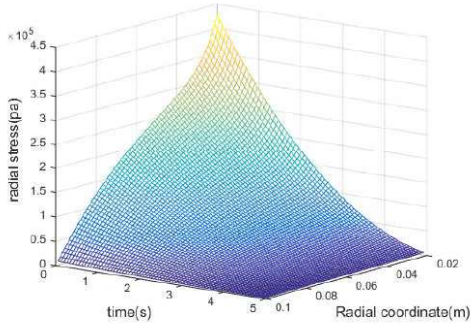

Figure 29: Three-dimensional profile of radial stress variation in terms of radial distance and time increase with a decelerated linear rotating speed for n = 1

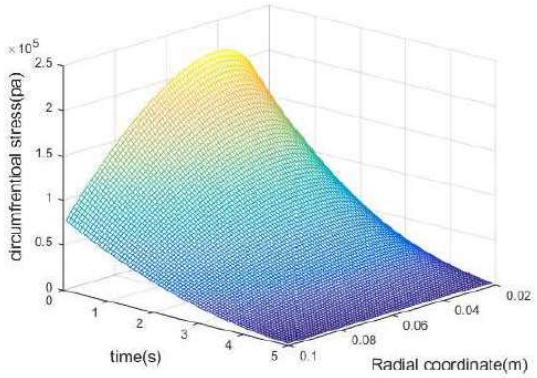

Fig. 30: Three-dimensional profile of circumferential stress variation in terms of radial distance and time increase with a decelerated linear rotating speed for n = 1

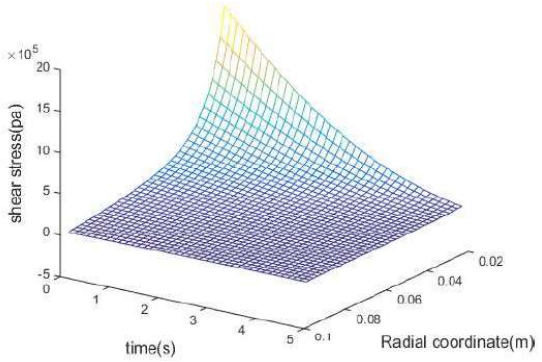

Fig.31: Three-dimensional profile of shear stress variation in terms of radial distance and time increase with a decelerated linear rotating speed for n = 1

It should be noted that the results for the distribution of obtained stresses and displacement in the linear decelerated rotational speed condition for the given period (0 s-5 s) are similar to the ones obtained for the accelerated rotating speed state.

The displacement and stress diagrams of the disk with the rotational speed in form of a quadratic function

In Fig. 32, the variation of the time function of accelerated quadratic rotational speed $\omega = 3.6t^2 + 10\ rad/s$ is shown in which the rotating speed of the disk increases with an increasing acceleration from ω = 10 rad/s to ω = 100 rad/s in a 5s period.

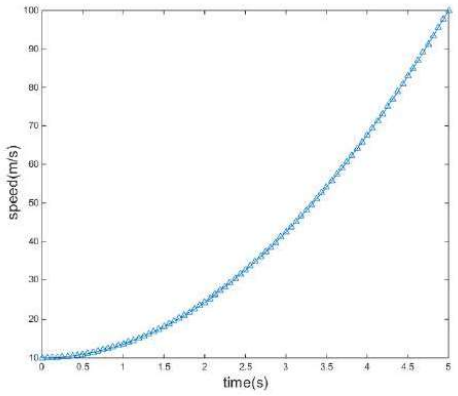

Figure 32: Variation of the rotating speed of the disk with an accelerated quadratic trend $\omega = 3.6t^2 + 10\ rad/s$

In Figs. 33, 34, 35, and 36, respectively, the three-dimensional model of variation for radial displacement, radial stress, circumferential stress, and shear stress are shown in terms of radial distance and time increase considering the accelerated quadratic function of $\omega = 3.6t^2 + 10\ rad/s$ for the rotating speed of the disk and for different values of FGM power index n = 0.2, 0.5, 1, 5, 20, 50 using the analytical method.

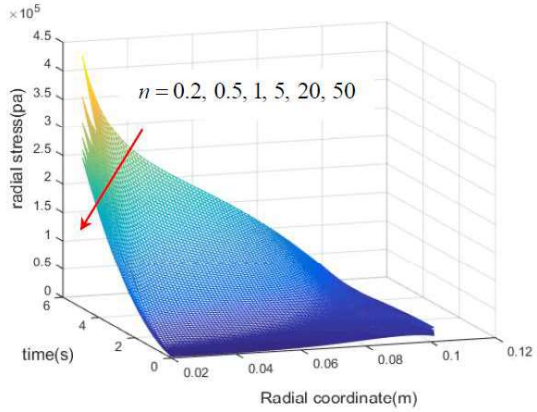

Figure 33: Three-dimensional profile of radial stress variation in terms of radial distance and time increase with an accelerated quadratic rotating speed $\omega = 3.6t^2 + 10\ rad/s$ for different values of n up to the fifth second (t = 5 s)

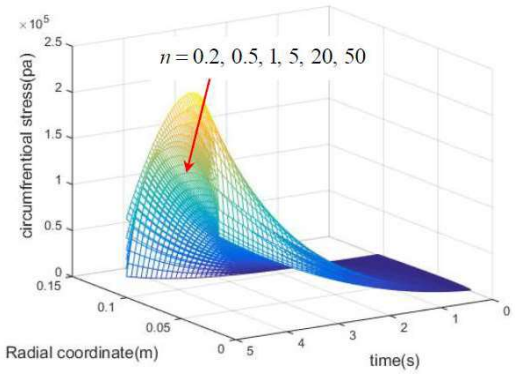

Figure 34: Three-dimensional profile of circumferential stress variation in terms of radial distance and time increase with an accelerated quadratic rotating speed $\omega = 3.6t^2 + 10\ rad/s$ for different values of n up to the fifth second (t = 5 s)

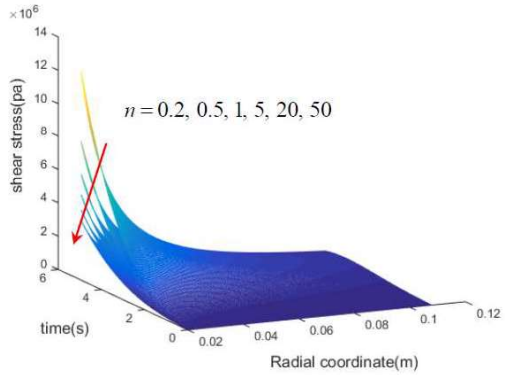

Figure 35: Three-dimensional profile of shear stress variation in terms of radial distance and time increase with an accelerated quadratic rotating speed $\omega = 3.6t^2 + 10\ rad/s$ for different values of n up to the fifth second (t = 5 s)

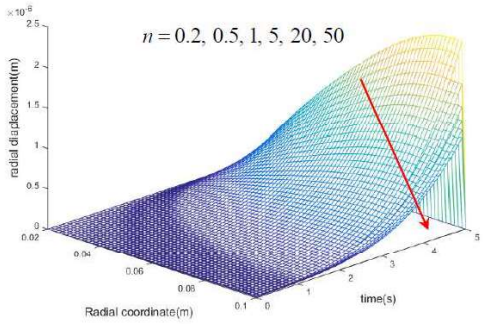

Figure 36: Three-dimensional profile of radial displacement variation in terms of radial distance and time increase with an accelerated quadratic rotating speed $\omega = 3.6t^2 + 10\ rad/s$ for different values of n up to the fifth second (t = 5 s)

The displacement and stress diagrams of the disk with the rotational speed in form of a square root function

In Fig. 37, the variation of the time function of accelerated square root rotational speed $\omega = 40.249t^{0.5} + 10\ rad/s$ is shown in which the rotating velocity of the disk increases with an increasing acceleration from ω = 10 rad/s to ω = 100 rad/s in a 5s period.

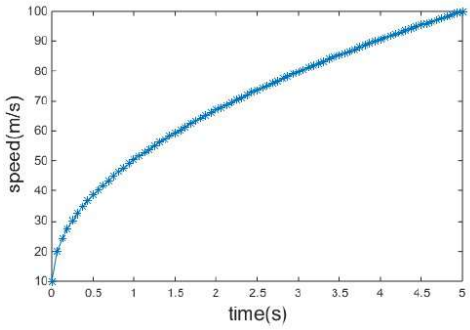

Figure 37: Variation of the rotating speed of the disk with an accelerated square root trend $\omega = 40.249t^{0.5} + 10\ rad/s$

In Figs. 38, 39, and 40, respectively, the three-dimensional profile f variation for radial displacement, radial stress, circumferential stress, and shear stress are shown in terms of radial distance and considering the accelerated square root function of $\omega = 40.249t^{0.5} + 10\ rad/s$ for the rotational speed of the disk and for different values of FGM power index n = 0.2, 0.5, 1, 5, 20, 50 using the analytical method.

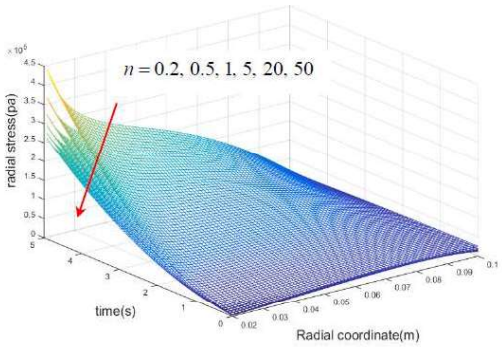

Figure 38: Three-dimensional profile of radial stress variation in terms of radial distance and time increase with an accelerated square root rotational speed $\omega = 40.249t^{0.5} + 10\ rad/s$ for different values of n up to the fifth second (t = 5 s)

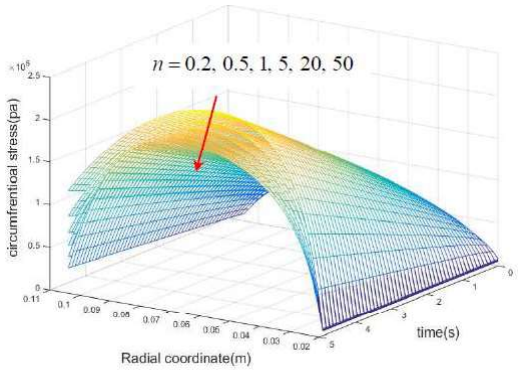

Figure 39: Three-dimensional profile of circumferential stress variation in terms of radial distance and time increase with an accelerated square root rotational speed $\omega = 40.249t^{0.5} + 10\ rad/s$ for different values of n up to the fifth second (t = 5 s)

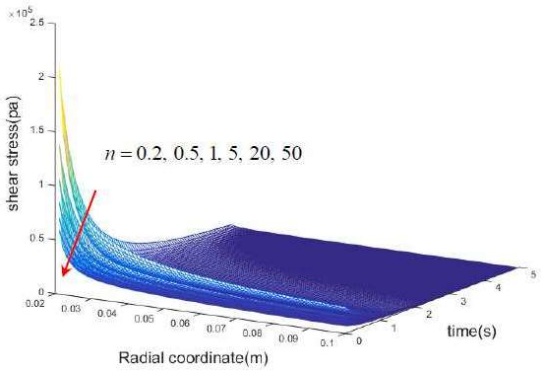

Figure 40: Three-dimensional profile of shear stress variation in terms of radial distance and time increase with an accelerated square root rotational speed $\omega = 40.249t^{0.5} + 10\ rad/s$ for different values of n

Results of plastic analysis for the rotating annular thin disk

In this section, firstly, to compare the results with other references and to justify the accuracy of the results in plastic analysis, for a constant thickness rotating annular disk considering Swift's hardening law [5] to simulate nonlinear hardening material the data in [5] with material parameter m = 2 are considered; and the developed computer mathematical code provided in environment of MATLAB was run. The obtained results for normalized displacement in radial direction $\bar{u}_r$ and normalized stresses $\bar{\sigma}_r$ and $\bar{\sigma}_\theta$ in the normalized radial position $\bar{r} = r/b$ = 0.5 are 0.81, 1.45, and 1.4, respectively. Again, these results show no differences compared to the analytical solutions of Eraslan [5].

Now, to analyze the plastic behavior model in this study, the geometric characteristics and mechanical properties of the disk with constant rotating speed are considered as follows [4]

$$a = 0.1\ m,\ b = 0.5\ m,\ \nu = 0.3,\ \omega = 450\ rad/s,$$

$$E(r) = 207\times10^{9}(r/b)^{n_1}\ Pa,\ \rho(r) = 7850\,(r/b)^{n_2}\ kg/m^3,$$

$$\sigma_y(r) = 235\times10^{6}\times(r/b)^{n_3}\ Pa,\ n_1 = n_2 = n,\ n_3 = n/4,\ n = 0.5,$$

In Fig. 41, the variation of plastic radial stress in terms of radial distance is indicated for the power index n = 0.5 using the Ludwig hardening law. It is observed that by increasing the radial distance, the value of radial stress increases from zero at the inner radius of the disk and reaches its maximum value at radius r = 0.04 m and then, it decreases to zero at the outer radius.

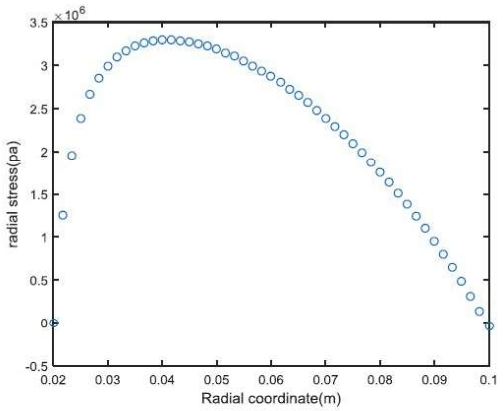

Figure 41: Variation of the plastic radial stress in terms of radial distance for n = 0.5 and constant rotational speed

In Fig. 42, the variation of plastic circumferential stress in terms of radial distance is indicated for the power index n = 0.5 using the Ludwig hardening law. It is observed that by increasing the radial distance, the value of circumferential stress decreases from its maximum value at the inner radius of the disk and reaches zero at radius r = 0.67 m and then, it increases to maximum value with negative sign at the outer radius.

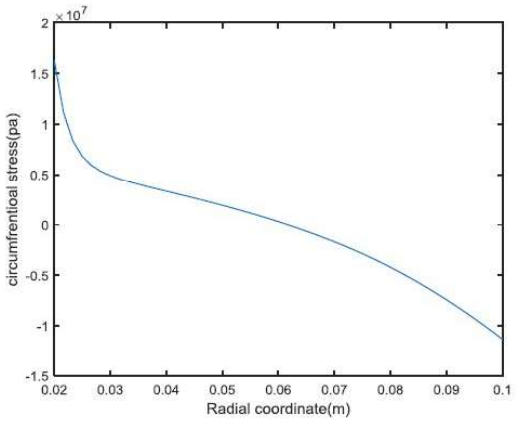

Figure. 42: The variation of the plastic circumferential stress in terms of radial distance for n = 0.5 and constant rotational speed

Conclusion

A summary of the results obtained in the elastic-plastic analysis of the annular rotating disk made of functionally graded material with different functions of rotational speed including constant rotating speed and time varying rotating speed such as the exponential, accelerated/decelerated linear, quadratic, and square root functions are as follows:

1. It was observed that the value of elastic radial stress decreases by increasing the radial distance so that the radial stress is decreased from its maximum value at the inner radius to zero at the outer radius for different values of inner radius of the disk. Also, the radial stress curves for different values of inner radius are often overlaid on each other.
2. The value of circumferential stress is increased by increasing the radial distance to a certain value, and then decreased in such a way that it reaches the minimum value at the outer radius.
3. The value of elastic shear stress decreases by increasing the inner radius, so that the shear stress in the inner radius decreases from the maximum value to zero at the outer radius.
4. It was observed that for constant value of the outer radius of the disk, the annular disk with small inner radius is exposed to greater elastic circumferential stress values than the annular disk with a large inner radius. Also, for the annular disk with different values of inner radius and constant outer radius, it was observed that the value of elastic radial stress at larger radial distances would often have the same values.

5. It was observed that by increasing the value of the power index of material *n*, the values of radial, circumferential, and shear stresses and radial displacement values are reduced for constant value of the inner and outer radius.
6. Using the Ludwig hardening law, it was observed that the value of plastic radial stress increases from zero at the inner radius of the disk and reaches the maximum value in a certain value of the inner radius, and then reaches zero at the outer radius with a decreasing trend.
7- It was observed that by increasing the radial distance, the value of plastic circumferential stress decreases from the positive maximum value at the inner radius so that it reaches zero in almost the middle radius of the disk, and then it is reduced again with a decreasing trend to reach the negative maximum value at the outer radius of the disk.

References

[1] Durodola, J.F., and Attia, O. "Deformation and stresses in FG rotating disks", Composite Science and Technology, Vol. 60, No. 7, pp. 987–995, 2000.
[2] Eraslan, A.N, and Argeso, H. "Limit angular velocities of variable thickness rotating disks" International Journal of Solids and Structures, Vol. 39, No. 12, pp. 3109–3130, 2002.
[3] Eraslan A.N., and Orcan, Y. "Elastic–plastic deformation of a rotating disk of exponentially varying thickness", Mechanics of Materials, Vol. 34, No. 7, pp. 423–432, 2002.
[4] Orcan, Y., and Eraslan, A.N. "Elastic–plastic stresses in linearly hardening rotating solid disks of variable thickness", Mechanics Research Communications, Vol. 29, No. 4, pp. 269-281, 2002.
[5] Eraslan A.N. "Von mises yield criterion and nonlinearly hardening variable thickness rotating annular disks with rigid inclusion", Mechanics Research Communications, Vol. 29, pp. 339-350, 2002.
[6] Eraslan A.N. "Elastic-plastic deformation of rotating variable thickness annular disks with free, pressurized and radially constrained boundary conditions", International Journal of Mechanical Science, Vol. 45, pp. 643–67, 2003.
[7] Zenkour, A.M. "Analytical solutions for rotating exponentially-graded annular disks with various boundary conditions", International Journal of Structural Stability, Vol. 5 No. 4, pp. 557-577, 2005.
[8] Eraslan A.N., and Akis, T., "On the plane strain and plane stress solutions of functionally
graded rotating solid shaft and solid disk problems", Acta Mechanica, Vol. 18, No. 1, pp. 43-63, 2006.
[9] Chen, J.Y., Ding, H.J., and Chen, W.Q. "Three-dimensional analytical solution for a rotating disc of functionally graded materials with transverse isotropy", Archive of Applied Mechanics, Vol. 77, No. 4, pp. 241-251, 2007.
[10] Zenkour, A.M. "Stress distribution in rotating composite structures of functionally graded solid disks", Jouranl of Materials Processing Technology, Vol. 209, No. 7, pp. 3511-3517, 2009.
[11] Asghari, M., and Ghafoori, E. "A three-dimensional elasticity solution for functionally graded rotating disks, Composite Structures, Vol. 92, No. 5, pp. 1092-1099, 2010.
[12] Callioglu, H., Bektas, N.B. and Sayer, M., Stress analysis of functionally graded rotating disks: analytical and numerical solutions, Acta Mechanica Sinica, Vol. 27, No. 6, pp. 950-955, 2011.
[13] Peng, X.-L., and Li, X.-F. "Elastic analysis of rotating functionally graded polar orthotropic disks", International Journal of Mechanical Science, Vol. 60, pp. 84-91, 2012.
[14] Peng, X.L., and Li, X.F. "Effects of gradient on stress distribution in rotating functionally graded solid disks", Journal of Mechanical Science and Technology, Vol. 26, No. 5, pp. 1483-1492, 2012.
[15] Zafarmand, H., and Hassani, B. "Analysis of two-dimensional functionally graded rotating thick disks with variable thickness", Acta Mechanica, Vol. 225, No. 2, pp. 453-464, 2013.
[16] Aleksandrova, A. "Exact deformation analysis of a solid rotating elastic-perfectly plastic disk", International Journal of Mechanical Sciences, Vol. 88, pp. 55-60, 2014.
[17] Zamani Nejad, M., Rastgoo, A., and Hadi, A. "Exact elasto-plastic analysis of rotating disks made of functionally graded material", International Journal of Mechanical Science, Viol. 85, pp. 47-57, 2014.
[18] Dai, T. and Dai, H.-L., "Investigation of mechanical behavior for rotating FGM circular disk with a variable angular speed", Journal of Mechanical Science and Technology, Vol. 29, No. 9, pp. 3779-3787, 2015.
[19] Callioglu, H., Sayer, M., and Demir, E. "Elastic-plastic stress analysis of rotating functionally graded disk", Thin-Walled Structures, Vol. 94, pp. 38-44, 2015.
[20] Zhenga, Y., Bahalooa, H., Mousanezhad, D., Mahdi, E., Vaziria, A., and Nayeb-Has H., "Stress analysis in functionally graded rotating disks with non-uniform thickness and variable angular velocity", International Journal of Mechanical Sciences, Vol. 119, pp. 283-293, 2016.
[21] Kalali, A.T., Hassani, B., and Hadidi-Moud, S., "Elastic-plastic analysis of pressure vessels and rotating disks made of functionally graded materials using the isogeometric approach", Journal of Theoretical and Applied Mechanics, Vol. 54, No. 1, pp. 113-125, 2016.
[22] Sharma, S., and Yadav, S., "Numerical solution of thermal elastic-plastic functionally graded thin rotating disk with exponentially variable thickness and variable density", Thermal Science, Vol. 23, No. 1, pp. 125-136, 2019.
[23] Ugural, A.C., "Theory of Plates and Shells", McGraw-Hill Book Company, 1999.
[24] Boresi, A.P., Chong, K. and Lee, J.D., "Elasticity in Engineering Mechanics, John Wiley & Sons, 2010.
[25] Johnson, W. and Mellor, P.B., "Engineering Plasticity", Ellis Horwood Limited, Van Nostrand Reinhold (UK), 1983.